AGU PUBLICATIONS

JGR

Journal of Geophysical Research: Oceans

RESEARCH ARTICLE

10.1002/2014JC009897

Key Point:
- Reduced refreezing of fractures in spring accelerates sea-ice drift

Correspondence to:
E. Olason,
einar.olason@nersc.no

Citation:
Olason, E., and D. Notz (2014), Drivers of variability in Arctic sea-ice drift speed, *J. Geophys. Res. Oceans*, *119*, 5755–5775, doi:10.1002/2014JC009897.

Received 10 FEB 2014
Accepted 8 AUG 2014
Accepted article online 19 AUG 2014
Published online 4 SEP 2014

Drivers of variability in Arctic sea-ice drift speed

Einar Olason[1,2] and Dirk Notz[1]

[1]Max Planck Institute for Meteorology, Hamburg, Germany, [2]Now at Nansen Environmental and Remote Sensing Center, Bergen, Norway

Abstract We explore the main drivers of seasonal and long-term variations in basin-scale Arctic sea-ice drift speed. To do so, we examine the relationship between the observed time-varying area-mean ice drift speed in the central Arctic and observed thickness and concentration as well as surface wind stress. Drift speeds are calculated from the positions of drifting buoys, thickness is based on submarine observations, concentration on satellite observations, and the wind stress comes from a global reanalysis. We find that seasonal changes in drift speed are correlated primarily with changes in concentration when concentration is low and with changes in thickness otherwise. The correlation between drift speed and concentration occurs because changing concentration changes how readily the ice responds to the synoptic-scale forcing of the atmosphere. Drift speed is correlated with neither concentration nor thickness in April and May. We show this behavior to be correlated with a decrease in the localization of deformation. This indicates that the increase in drift speed is caused by newly formed fractures not refreezing, leading to an overall reduced ice-cover strength without a detectable change in ice concentration. We show that a strong long-term trend exists in months of relatively low ice concentration. Using our analysis of the seasonal cycle, we show that the trend in concentration drives a significant portion of the drift-speed trend, possibly reinforced by a trend in cyclone activity. Hence, the trend in drift speed in this period is primarily caused by increased synoptic-scale movement of the ice pack.

1. Introduction

The main features of the large-scale drift pattern of Arctic sea ice have been well-established for decades: ice circulates as part of the Beaufort Sea Gyre and is transported out of the Arctic through Fram Strait by the Transpolar Drift Stream [*Gordienko*, 1958; *Colony and Thorndike*, 1984]. It is also well-known that this system displays substantial spatiotemporal variability [*Proshutinsky and Johnson*, 1997; *Martin and Gerdes*, 2007]. A long-term trend and a seasonal cycle in the mean central Arctic drift speed were identified by *Rampal et al.* [2009]. The long-term trend was also confirmed by *Spreen et al.* [2011], *Vihma et al.* [2012], and *Kwok et al.* [2013], all of which conclude that wind forcing can be excluded as the main driver for the drift-speed increase. In the most recent of these works, *Kwok et al.* [2013] combined satellite and buoy data to study basin-wide trends between 1982 and 2009. They found considerable variability in ice drift linked to changes in Arctic Oscillation and were also able to link regional increases in drift speed to a decrease in multiyear sea-ice cover.

While seasonal and long-term changes in Arctic sea-ice drift are hence well established, the underlying drivers of these changes have so far not been clearly identified. Closing this gap in our understanding is the primary aim of the present contribution, in which we combine observations and our understanding of the basic physics to examine the drivers of the changing large-scale sea-ice drift in the Arctic on both seasonal and longer time scales.

For our analysis, we build on the established physics that governs the dynamics of drifting sea ice. Much of our understanding in this respect derives from the experiments and analysis of the Arctic ice dynamics joint experiment (AIDJEX). An important outcome of this experiment was the elastic-plastic sea-ice model of *Coon et al.* [1974]. In this model, the momentum of the ice is determined by surface drag delivered by atmosphere τ_a and ocean τ_w, the Coriolis force, the ocean surface tilt, and the ice internal stress given by the divergence of the stress tensor σ:

$$\frac{D}{Dt}(m\vec{u}) = \vec{\tau}_a + \vec{\tau}_w - mf\vec{k}\times\vec{u} - mg\vec{\nabla}H - \nabla\cdot\sigma. \quad (1)$$

Here the term on the left hand side is the total derivative of the mass, m times velocity $\vec{u}$. A scale analysis shows that on a time scale longer than a few hours the total derivative, Coriolis force and sea-surface-tilt terms can be neglected [see e.g., *Leppäranta*, 2005]. On the time scales that we consider here, this then leaves changes in the atmospheric drag, in the oceanic drag, and in the internal friction as the possible drivers of the observed changes in sea-ice drift speed.

The drag and internal friction can, however, not be reliably estimated at the large spatial scale that we consider here. We therefore examine the variation of large-scale observations of sea-ice concentration, sea-ice thickness, and wind speed that to first-order govern the variation of the terms in the force balance as follows: when concentration is high and constant, large-scale ice strength increases with increasing ice thickness h, most likely proportionally to $h^{3/2}$ [*Rothrock*, 1975; *Hopkins*, 1998; *Lipscomb et al*., 2007]. With decreasing concentration, ice strength reduces rapidly [see e.g., *Rothrock*, 1975; *Hibler*, 1979, 1980]. *Hibler* [1979] approximated this behavior using an exponential function, while *Rothrock* [1975] suggests a piecewise linear function with a similar shape. In both cases, the authors assume that once the concentration drops below about 0.8 the ice is in free drift. Both the ice–atmosphere drag and the ice–ocean drag increase as concentration decreases because of an increased form drag at the edges of ice floes. *Lüpkes et al*. [2013] suggest a linear relationship between the open water fraction and ice-atmosphere drag coefficient, while *Lu et al*. [2011] show that a more complicated relationship governs the ice-ocean drag because of wake effects. The atmospheric and oceanic drags are additionally proportional to the square of the wind speed and the differential ice-ocean velocity, respectively.

Because of these relationships, changes in the observable quantities sea-ice concentration, sea-ice thickness, wind speed, and oceanic currents are the most fundamental drivers of any changes in drift speed as described by equation (1), and they consequently form the core of our analysis. Due to limited amount of observations we can, however, not consider the oceanic forcing, even though this is an important part of the force balance. We expect the underlying geostrophic currents to show little seasonal variations and that long-term variations be driven by the atmosphere, which would make its inclusion here unnecessary. This is, however, not explicitly demonstrated in the text.

Our choice of the three principle variables ice thickness, ice concentration, and wind speed is based on the classical description of sea-ice dynamics outlined above. However, it turned out that for understanding the entire seasonal cycle of sea-ice drift we also have to consider changes that occur in the fracturing of the ice cover. This suggests that the observed patterns and trends in Arctic sea-ice drift are not fully consistent with our classical understanding of its drivers [cf., *Coon et al*., 2007]. To take fracturing into account, we use satellite observations of ice motion, from which we can calculate the degree of localization of the deformation of the ice cover.

We use a central-Arctic wide spatial average of all observational fields, which allows us to compare data from different sources in a straight forward manner. Our approach implies that we treat the Arctic ice cover as a single physical entity, integrating over small-scale aspects of its internal structure and focusing on temporal changes of the integrated behavior. We do not explicitly discuss the drivers of the observed changes in concentration and thickness, noting, however, that they are obviously related.

Much of our study rests on analyzing correlations between drivers and response. While obviously correlation does not necessarily imply causality, combining our physical understanding of the system with a correlation analysis can nevertheless allow us to test the robustness of the physical understanding. For example, if our understanding says that a certain process drives a certain response, and we find no correlation between driver and response, we know that something is wrong with our understanding. In contrast, if out of several possible drivers only one shows a clear correlation to a specific signal, this strongly indicates that the other drivers are of minor importance.

This paper is organized as follows: in section 2, we give an overview of the data used. In section 3, we analyze how wind, ice concentration, ice thickness, and ice fracturing shape the seasonal cycle in drift speed. This is then followed by a section analyzing the long-term trend in sea-ice drift speed. We discuss our results in section 5, where we also explain some of the discrepancies between observed and CMIP3 modeled drift speed [*Rampal et al*., 2011]. We present our conclusions in section 6.

2. Data and Methods

We calculate drift speeds using data from the International Arctic Buoy Programme (IABP) that maintains a network of drifting buoys in the Arctic Ocean for operational and research purposes. We use their data covering the period 1979–2011, consisting of 658,269 measurements of position, pressure, and temperature from 910 buoys. To allow for an analysis of drift speed versus ice-thickness data, we use only buoy positions from within the data-release area of the submarine thickness data discussed below. The selection is made using the spatial coordinate system from *Rothrock et al*. [2008]. This reduces the number of reported buoy positions to 316,855. The position data are provided every 12 h and we use the buoy displacement over this interval to calculate the 12 hourly mean speed. We eliminate observations showing unrealistic speed, but our results are not sensitive to this procedure. Discarding speeds larger than 90 km/d leaves 310,409 usable speed values.

For our analysis, it is useful to filter out the direct response of drift speed to changes in the wind forcing. We do this by normalizing the central Arctic mean monthly climatology of drift speed with the central Arctic mean monthly climatology of the friction speed based on the ERA-interim reanalysis surface stress [*Simmons et al*., 2006]. The friction speed is calculated as $u^* = \sqrt{\tau/\rho}$, where τ is the surface stress and $\rho \approx 349/T$ kg/K/m^3 is an approximation for atmospheric density based on atmospheric temperature. The surface stress is a climatological monthly mean of the 12 hourly instantaneous surface stresses provided.

Using the central Arctic mean, climatology is consistent with our usage of Arctic-wide integral values only. It is also a reasonable first approximation, since *Thorndike and Colony* [1982] and *Thomas* [1999] have shown a strong correlation between geostrophic wind speed and ice drift-speed, while using the friction speed additionally takes changes in atmospheric stability implicitly into account.

To filter out synoptic-scale forcing, we also calculate the fortnightly mean speed of each buoy, assuming the synoptic time scale to be about a week. To calculate the fortnightly mean speed, we consider each reported buoy position within the data-release area and search for that buoy's position after 2 weeks. If that position is also within the data-release area, we divide the buoy displacement by 2 weeks, giving a mean speed over the period. The resulting mean speed is given a time stamp 1 week after the time stamp of the first observation. This time stamp is used when calculating monthly and climatological means.

Both the 12 hourly and fortnightly mean speeds are averaged spatially and temporally to give a time series of the monthly mean drift speed within the submarine data-release area, and then further averaged to produce a monthly climatology. The uncertainty of the monthly means, due to the small sample size, is estimated using the same bootstrap method as *Rampal et al*. [2009]. This method estimates the constants A and λ in the equation

$$\Delta\bar{u} = A\bar{u}n^{-\lambda}, \tag{2}$$

where $\Delta\bar{u}$ is the uncertainty of the mean speed $\bar{u}$ and n is the number of observations used to calculate $\bar{u}$. The estimate is derived by repeatedly selecting random subsets of speeds from each month of observations and then calculating the standard deviation of the mean of these subsets. Using different sample sizes, A and λ are estimated using equation (2).

Our analysis gives $A = 0.7$ for the 12 hourly means, $A = 0.5$ for the fortnightly ones, and $\lambda = 0.5$ for both. Finding $\lambda = 0.5$ is consistent with the central limit theorem, indicating a random distributions of speeds in space and time. Our estimates of A and λ differ from those of *Rampal et al*. [2009], who found that $A = 0.6$ and $\lambda = 0.3$ (for the 12 hourly means). A possible reason for this difference is differences in sampling frequency, since *Rampal et al*. [2009] use both 3 hourly and 12 hourly positions, while we only had access to 12 hourly positions. This indicates that the majority of velocity correlations between buoys occurs because of inertial oscillations, which are not resolved by the 12 hourly data. Our results, in any case, are not sensitive to the different uncertainty estimates.

In addition to the buoy data, we also use sea-ice drift data based on satellite observations [*Fowler et al*., 2013]. For the main part of the paper, we use drift speeds calculated from images from the SSM/I, SSMIS, and AVHRR sensors. This data are available from late July 1981 to the present time and gives daily velocity fields. The difference between daily and 12 hourly speeds when using the buoys is about 0.3 km/d, so we can expect a similar reduction in speed here due to the reduced sampling frequency. We do not use the

Table 1. Satellite-Based Concentration Products Used

Product	Sensor(s)	Period Used Here
Bootstrap	SMMR, SSM/I, and SSMIS	1979–2011
NASA team	SMMR, SSM/I, and SSMIS	1979–2011
ASI (SSMI)	SSM/I and SSMIS	1992–2011
ASI (AMSR-E)	AMSR-E	2003–2011
MPF	MODIS	2000–2011

satellite data during the melt season since drift speeds calculated from passive microwave observations are considered unreliable during that time [*Fowler et al*., 2013]. We treat the individual drift vectors provided as independent observations and process the resulting speed in the same way as we did for the buoy speeds. Appendix B contains a closer look at the data provided by *Fowler et al*. [2013] and justifies using only the SSM/I, SSMIS, and AVHRR based drift speeds for the rest of the paper, and not the combined product provided by *Fowler et al*. [2013].

For an improved understanding of how the ice cover deforms throughout the year, we calculate the total strain rate, based on the shear and divergence deduced from observations using the RADARSAT Geophysical Processor System (RGPS) [*Kwok et al*., 1990]. This data are provided on a 10×10 km grid every 3 days for all months of the year, except August, September, and October. The observations are available from early November 1996 to the end of April 2008. We use all observations from within the submarine data-release area where the RGPS data are available, which is the case south of 87.2°N, west of approximately 85°N, and east of approximately 140°E.

The sea-ice concentration data we use is primarily derived from passive microwave satellite observations using the AMSR-E Bootstrap algorithm [*Comiso*, 2000]. The NSIDC also provides concentrations derived using the original NASA Team algorithm, which we use for comparison here. Sea-ice concentration derived from the original NASA Team algorithm has been shown to be inferior to the enhanced NASA Team algorithm [*Markus and Cavalieri*, 2000], which in turn gives comparable results to the AMSR-E Bootstrap algorithm [*Comiso and Parkinson*, 2008]. We also use results from the ASI algorithm for further comparison, applied to both SSM/I–SSMIS observations and to AMSR-E observations [*Kaleschke et al*., 2001; *Spreen et al*., 2008].

Ice concentration inferred from any of these passive-microwave algorithms is less reliable in summer time when melt ponds are present [cf., *Meier and Notz*, 2010]. The microwave signature of these melt ponds is very similar to that of open water, which is why the algorithms in summer initially see too small an ice cover since they interpret melt ponds as open water. This systematic bias is compensated for to various degrees by different algorithms, but the reliability of this compensation is not clear. To explore the impact of possible biases caused by melt ponds in passive microwave data, we additionally use ice concentration derived from visual MODIS imagery [*Rösel et al*., 2012]. This data set allows us to quantify the distribution of bare ice, ponded ice, and open water individually. The data are available as weekly averages from May to the first week in September, but we combine these into monthly averages and discard the September data since it only covers the first week and is hence not representative for a monthly mean.

We use monthly mean concentration data and average the data spatially to give a time series of monthly mean concentration in the ice covered portion of the submarine data-release area, and then average in time to give a monthly mean climatology. The temporal span of the satellite data is summarized in Table 1. For the Bootstrap algorithm, which shows little variation in concentration in the central Arctic, we fill the satellite "pole hole" with constant concentration of $\bar{A}=0.988$ (see appendix A for details). This is not feasible for the other algorithms since they give too high variability in sea ice concentration in the central Arctic. For these algorithms, the pole-hole area is left out when calculating the spatial average. Filling the pole hole has no significant effects on our concentration calculations, but doing so allows us to still use data within the satellite pole hole from the other data sets.

For thickness estimates, we primarily use the multiple regression model of *Rothrock et al*. [2008]. They used data from 34 U.S. Navy submarine cruises to construct a multiple regression model of the ice draft within the data-release area of the cruises. This area is an irregular polygon approximately demarcated by the exclusive economic zone of the countries bordering the Arctic Ocean, with the exception of that of the United States, where the polygon reaches the coast (see Figure 1). The data set spans the years 1975–2000 and contains 2203 records of mean drafts, with most of the measurements taken in spring (MAM) and autumn (SON). We convert the draft into thickness using the same climatological method as *Rothrock et al*. [2008].

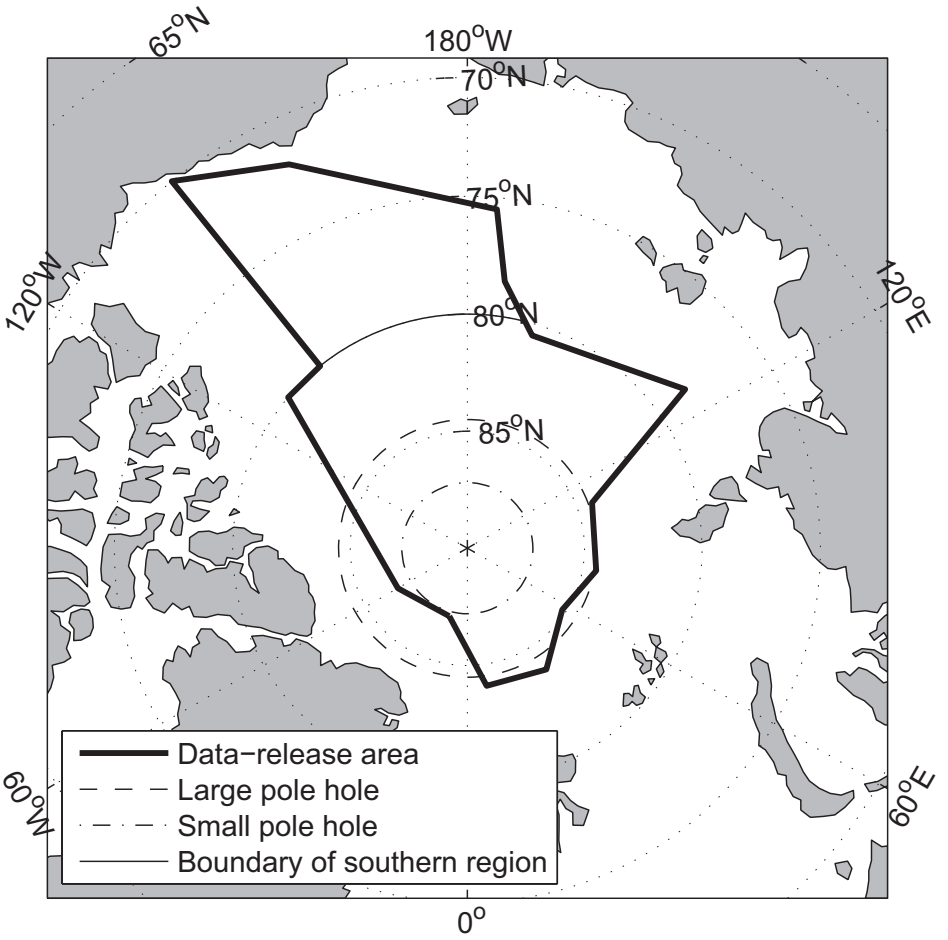

Figure 1. The data-release area of the submarine ice draft data (thick solid line). The passive microwave satellite data "pole holes" are also included, the larger hole being relevant from 1979 to August 1987 and the smaller after that. A thin solid line is drawn at 80° N indicating the northern boundary of the southern region discussed in the text.

In addition to the *Rothrock et al*. [2008] multiple regression model, we also consider the results of the PIOMAS reanalysis model [*Zhang and Rothrock*, 2003] which have been evaluated against several independent observations [*Schweiger et al*., 2011]. In particular, the seasonal cycle of the *Rothrock et al*. [2008] model is poorly constrained by the observations and so we expect the PIOMAS model to give more accurate results in that respect. For the long-term trend in thickness, we also take the more recent ICESat record into account [*Kwok and Rothrock*, 2009].

3. Seasonal Cycle of Drift Speed

In this section, we discuss the seasonal cycle seen in the climatological monthly mean drift speed. This seasonal cycle is shaped by either the applied forcing, the ice response, or both. In the following, we first analyze a possible impact of seasonality in the forcing, and then turn to a seasonality in the response.

3.1. Seasonality in the Forcing

Seasonality in the mean wind forcing cannot be the primary cause for the seasonality in drift speed, since the seasonal cycle in mean friction speed lags after the drift speed, with a maximum in the cross correlation at 1 month lag (see Figure 2). For our analysis of the seasonal cycle, we find it helpful to filter out the response to changes in mean wind forcing and will therefore use the normalized drift speed introduced in section 2 for the remainder of this section. We note that the data retain their seasonal characteristics after normalization (see Figure 3).

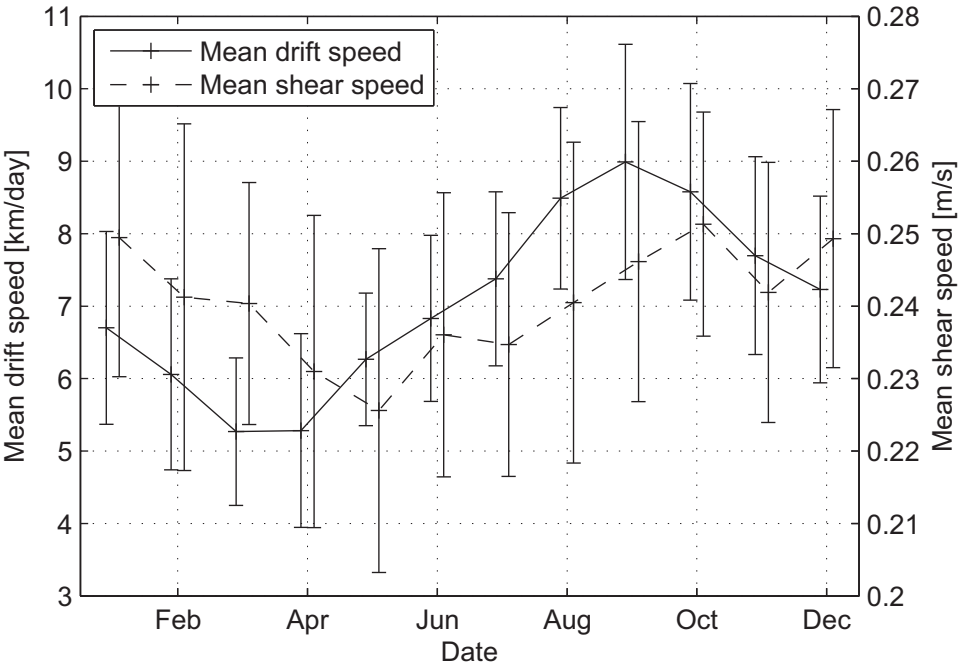

Figure 2. A monthly climatology and standard deviation of the mean ice drift speed (12 hourly) and mean friction speed in the submarine data-release area from 1979 to 2010. The *x* position of the drift data is shifted by +3 days and that of wind by −3 days to improve presentation of the error bars, which show the standard deviation of the monthly means.

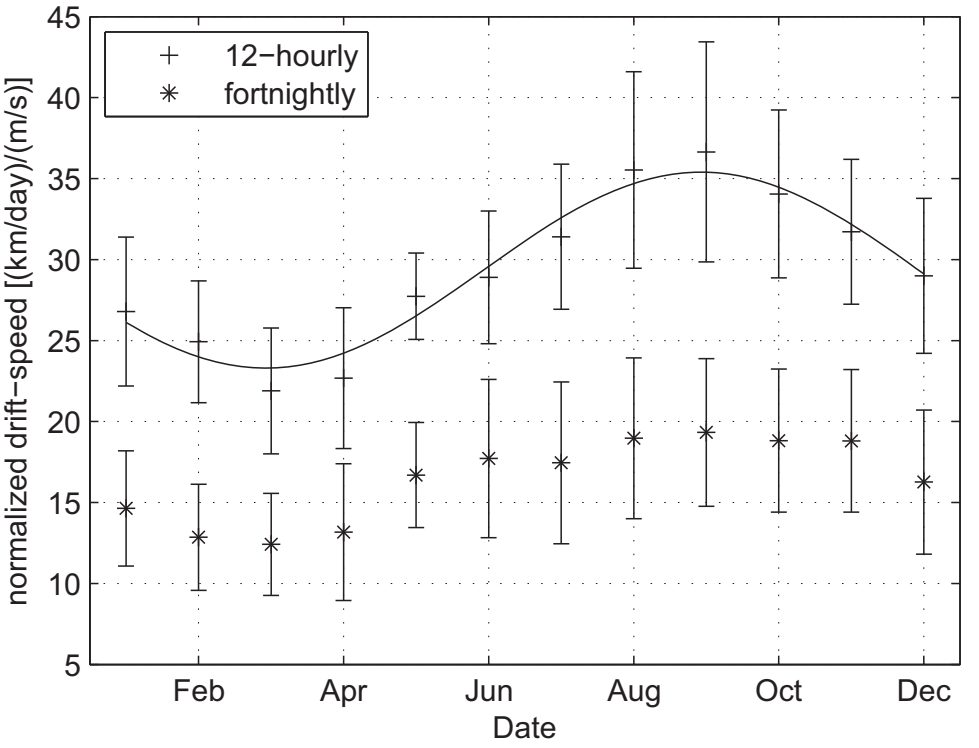

Figure 3. Seasonal cycle of normalized drift speed within the submarine data-release area based on 12 hourly data and fortnightly data. A sinusoidal fit for the 12 hourly data is also shown, as well as the standard deviation of the data. The error bars show the standard deviation of the monthly means.

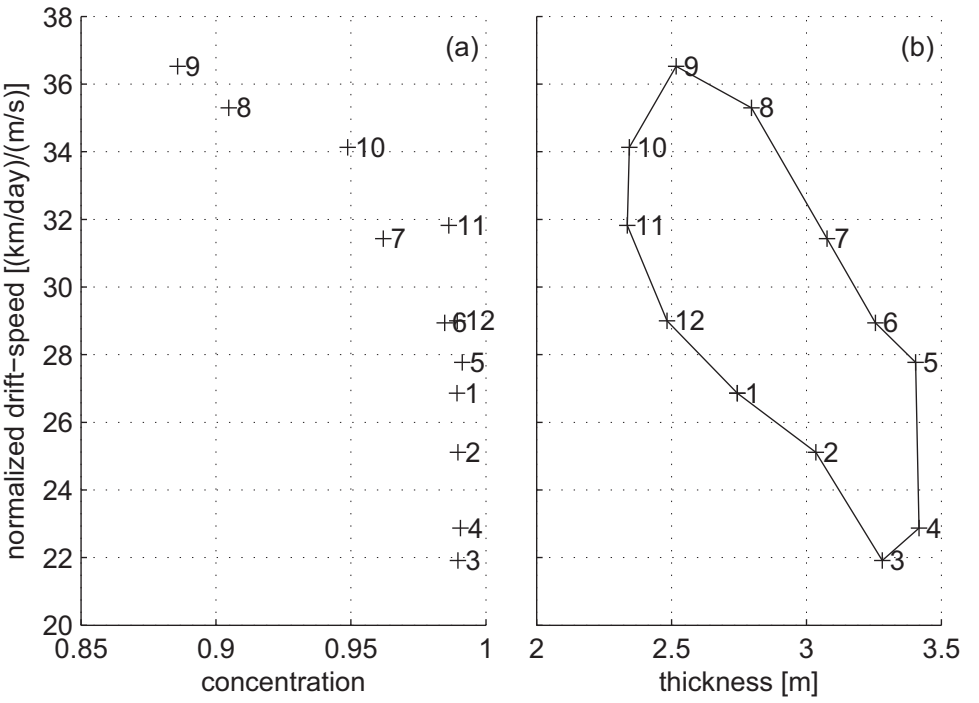

Figure 4. Scatter plots of monthly climatologies of (a) concentration using the Bootstrap algorithm results and (b) thickness based on the submarine observations against 12 hourly normalized drift speed. The numbers denote the month (1 for January etc.) and the crosses are the actual data points.

We can consider the wind forcing to be composed of the mean wind forcing and the synoptic-scale forcing. A seasonal cycle in the synoptic-scale forcing could drive the seasonal cycle in drift speed, even if the seasonality in the mean wind cannot as discussed in the previous paragraph. The seasonality of the synoptic-scale forcing is most readily inferred from an analysis of cyclone activity. It is well known that a passing cyclone will decrease the ice-cover fraction [see e.g., *Zwally and Walsh*, 1987; *Maslanik and Barry*, 1989; *Holt and Martin*, 2001] and increase the mobility of the ice floes [*Brümmer and Hoeber*, 1999]. An increase in cyclone activity in the Arctic from May to August and then a decrease from September to November could hence explain the observed pattern in 12 hourly drift speed. *Zhang et al*. [2004] have composed a comprehensive overview of the climatology and variability of Arctic cyclones. They found cyclone intensity north of 70°N to decrease from January to July and then start to increase again. They also found cyclone duration in the same region to show little variation (see their Figure 3). This is inconsistent with the observed increase in drift speed from June to August and decrease from September to November. We therefore conclude that seasonality in cyclone activity and hence the seasonality of the synoptic-scale forcing cannot explain the observed variability in sea-ice drift speed.

3.2. Seasonality in the Response

Having excluded a dominating role of seasonality in the forcing, the seasonality in drift speed must stem from a seasonality in the ice response to the applied forcing. The main variables controlling the ice response are concentration and thickness. As described in the introduction, for concentrations between roughly 0.8 and 1, variations in concentration greatly affect the ice cover strength, and thus the ice drift speed. The role of ice thickness only becomes dominant when concentration is high and constant.

In the following, we therefore consider the periods of low concentration between June and November separately from the period of high concentration from December to March. Our working assumption is that during the former period changes in sea-ice concentration most strongly affect drift speed, while in the latter period, where concentration is almost constant, changes in ice thickness become more relevant. In addition, we separately consider the months April and May, since the drift speed changes drastically during these months with no clear concurrent change in either thickness or concentration.

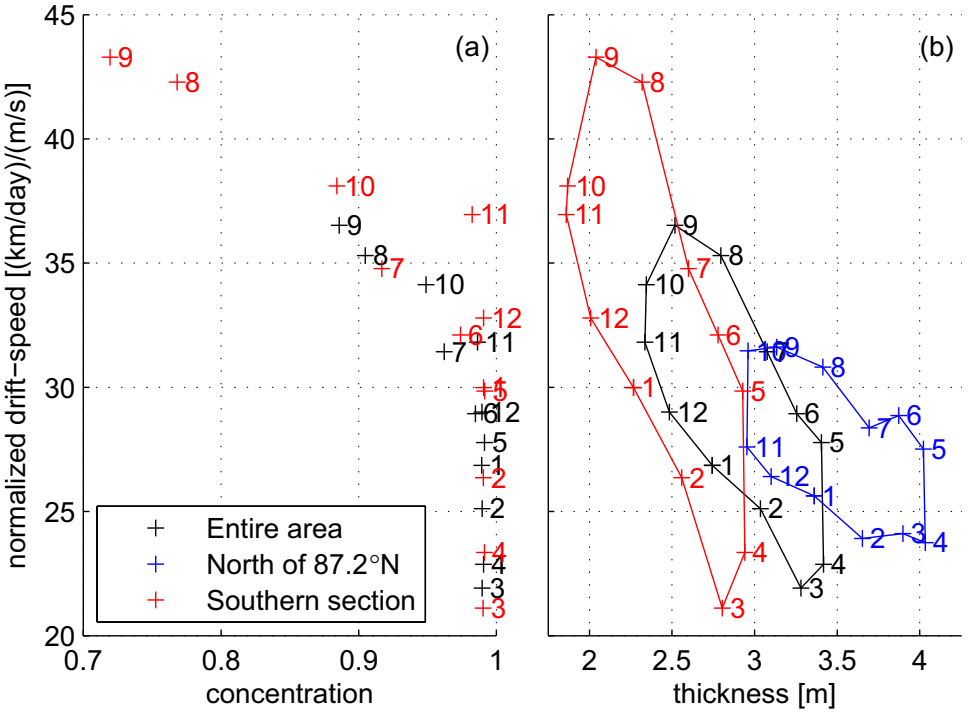

Figure 5. Scatter plots of monthly climatologies of (a) concentration using the Bootstrap algorithm results and (b) thickness based on the submarine observations against 12 hourly normalized drift speed. The numbers denote the month (1 for January etc.) and the crosses are the actual data points. See text and Figure 1 for definitions of the two sections. No concentration data are available for the northern section due to the satellite pole hole.

3.2.1. June to November

During the period June to November, the mean concentration in the central Arctic varies within the range 0.8 to slightly below 1. We hence expect concentration to have a major impact on normalized sea-ice drift speed. This is consistent with the high anticorrelation of $\rho = -0.978$ that we find between the monthly and spatial mean concentration and speed during this period (Figure 4a). A least squares fit between normalized drift speed and ice concentration gives an change in normalized drift speed of -64 ± 41 (km/d)/(m/s) per unit change concentration.

The robustness of this correlation might, however, be jeopardized by the uncertainty in sea-ice concentration from passive-microwave products during summer time, as discussed in section 2. To ascertain the robustness of our analysis, we consider two subsections of the data-release area, each with relatively high and low concentration, respectively, as well as different algorithms for the satellite data.

For the two subsections, we separate the data-release area into a southern section south of 80°N with 112,671 buoy positions, and a section inside the small satellite pole hole, or north of 87.2°N, with 40,470 buoy positions. The southern section is chosen to demonstrate the relationship between normalized drift speed and concentration where concentration is relatively low, while the northern section is chosen to demonstrate the relationship between normalized drift speed and thickness where we can assume concentration is relatively high and nearly constant throughout the year. The resulting scatter plot is shown in Figure 5a.

The relationship between normalized drift speed and concentration remains the same in the southern section as it was for the entire area, despite the higher drift speeds and lower concentration that are present in the southern region. A least-squares fit from June to November gives for the southern region a change in normalized drift speed of -37 ± 24 (km/d)/(m/s) per unit change in ice concentration, slightly less than we found for the entire region.

Moving the northern boundary of the southern section further south (not shown) increases primarily the difference between the melt and freeze-up portions of the low concentration regime, but does not reduce

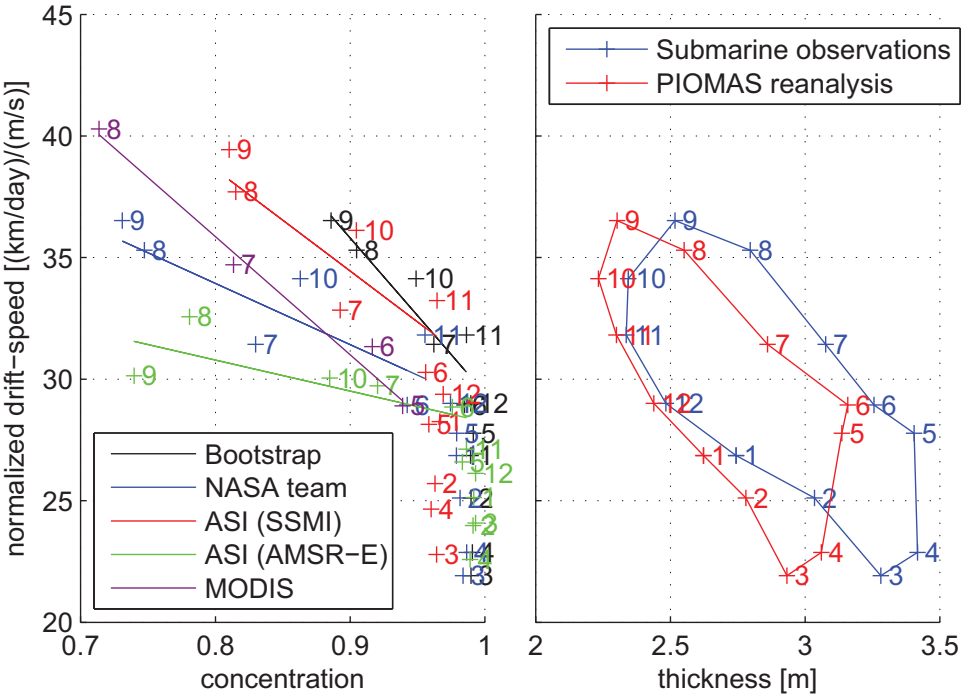

Figure 6. Scatter plots of monthly climatologies from within the submarine data release area of (a) concentration against 12 hourly normalized drift speed for different satellite products and (b) thickness against 12 hourly normalized drift speed for the submarine observations and PIOMAS reanalysis results. The numbers denote the month (1 for January etc.) and the crosses are the actual data points. The straight lines in (a) are liner fits for the months June to November.

the mean concentration by a considerable amount. The difference between melt and freeze-up increases when scaling with the 10 m wind speed instead of the friction speed, indicating that near-surface stability during the melt is affecting the ice-atmosphere drag. Similarly, the ice-ocean drag will be affected by the melt, but this is more difficult to quantify, as discussed below. We have no satellite observations of concentration for the northern region. We can, however, assume the concentration to be always high and nearly constant there (see appendix A) and we consequently do not expect to see a clear relationship between normalized drift speed and concentration there.

So far we have focused on sea ice concentration data for which the Bootstrap algorithm is used to convert brightness temperatures observed by satellites to ice concentration. As stated before, the accuracy of the various algorithms used to convert brightness temperatures to concentration is not well known, and a thorough error estimation is well outside the scope of this paper. To test the robustness of our analysis in light of the uncertainty in the satellite-derived sea-ice concentration, we repeated our analysis of normalized drift speed as a function of concentration for the NASA Team algorithm, the ASI algorithm applied to SSM/I and AMSR-E data, and the MODIS-based melt-pond fraction (MPF) algorithm (Figure 6a). The MPF and two ASI-based products are only available for the more recent part of the time period covered by the Bootstrap and NASA Team data (see Table 1), causing higher mean for the normalized drift speed for the MPF and ASI-based products.

The different satellite products show considerable variations in reported concentration, but all products show a qualitatively similar relationship between the normalized drift speed and concentration. The correlation between drift speed and concentration, when using the NASA Team algorithm is $\rho=-0.835$, compared to $\rho=-0.912$ when using the Bootstrap algorithm. For the ASI algorithm applied to SSM/I data and AMSR-E data, this correlation is $\rho=-0.871$ and $\rho=-0.771$, respectively, and for the MPF product it is even $\rho=-0.999$. It should be noted, however, that the Bootstrap and NASA Team algorithms use data from a considerably longer period than the others. It is especially interesting that the linear relationship holds particularly well for the MPF product, since that product is not affected by the uncertainty in sea-ice concentration resulting from melt ponds. This is because the MPF product uses different spectral bands than the

passive microwave sensors and can therefore separately identify melt ponds, open water, and ice. [*Rösel et al*., 2012]. The MPF product is, however, only available during the melt season.

Overall, the robustness of our findings across a variety of satellite products gives additional support to the notion that the expected relationship between sea-ice concentration and normalized drift speed is indeed observed and not simply an artifact arising from uncertainties in sea-ice concentration data. For every product considered here, there is a linear relationship between concentration and normalized drift speed, from June to November. The concentration reported by the different satellite products differs considerably, and so do the slopes of the lines in Figure 6. The fact that the linear relationship holds, despite these differences indicates that the linear relationship is a robust one.

In addition to changes in concentration, changes in thickness could also influence the ice drift speed during the period of low concentration that we currently consider. However, a possible contribution of ice thickness to the observed variation in drift speed between June and November must be quite small, since we find an inconsistent relationship between ice thickness and normalized drift speed during this period (Figures 4b, 5b, and 6b). Independent of region or data source, we find that from July to September an increase in ice thickness goes along with an increase in normalized drift speed, while from September until November the drift speed decreases rapidly with almost no change in ice thickness. This makes a physical relationship between the observed changes in ice thickness and normalized drift speed unlikely. We also know that the ice cover progressively looses its ability to transmit stresses from mid-May toward summer [*Stern and Lindsay*, 2009]. This means that there is progressively less deformation of ice, which is the only way in which ice thickness can affect drift speed. The anticorrelation between normalized drift speed and thickness from May to September is therefore unlikely to be caused by thickness changes driving drift speed changes in that period.

When it comes to the ice-ocean drag, seasonal changes in the stability of the upper ocean may also play a role. It is well known that a layer of fresh water on top of more saline water can cause so-called dead water [*Ekman*, 1904], where internal waves form at the bottom of the fresh water layer, increasing the drag felt at the ocean surface. *Waters and Bruno* [1995] showed that introducing such a fresh water layer may cause as much as a fivefold increase of the ice-ocean drag. If we could include this effect in the normalization of the ice drift speed, we would expect to see higher normalized drift speeds at the peak of the melt season. We cannot quantify this effect at the moment, but we can speculate that this could cause the normalized drift speed in June and July to be higher and more in line with the relationship between drift speed and concentration observed from August to November.

Having excluded the seasonal cycle in the synoptic forcing and changes in ice thickness as major drivers of changes in mean drift speed during the period June to November, changes in ice concentration remain as the most likely physical parameter that determines the evolution of sea-ice drift speed during periods of comparably low ice concentration. Changes in atmospheric stability are unlikely to play a role when the ice cover is not closed and changes in ocean stratification are only likely to be important during melt, through the dead-water effect discussed above.

To understand in more detail how this relationship between sea-ice concentration and mean sea-ice drift speed works, we compare the seasonal cycle of the normalized drift speed based on 12 hourly buoy displacement with that based on fortnightly buoy displacements (Figure 3). The 12 hourly data represents the best available temporal resolution, while the fortnightly data filters out synoptic-scale forcing. Using different sampling intervals gives a rapid seasonally nonuniform decrease in speed going from 12 hourly data to fortnightly. Choosing larger sampling intervals gives a small reduction in speed that is mostly uniform over the year (not shown).

We find that the fortnightly data have both reduced amplitude and seasonality compared to the 12 hourly data. Calculating the ratio of the two, we find that synoptic-scale forcing drives on average 45% of the observed ice drift speed. This fraction is, however, not constant. In particular, the fortnightly drift speed remains nearly constant from May to November while the 12 hourly drift speed shows a strong seasonal signal during these months. Hence, synoptic-scale forcing must be crucial for shaping the observed seasonal cycle.

However, since we have already shown that seasonal changes in the synoptic-scale forcing cannot shape the seasonal cycle by themselves, their importance for shaping the seasonal cycle must lie in the ice

response. As discussed, the ice response depends from June to November primarily on concentration, which hence links the synoptic-scale variability to changes in ice drift speed. When concentration is low the ice is free to move back and forth as cyclones pass over, but when concentration is high, the ice internal stresses dampen this response. The variability in ice drift speed from June to November is thus primarily caused by variability in the ice cover's mobility through changes in ice concentration, and not by changes on a time scale larger than the synoptic one.

3.2.2. December to March

We now consider the period from December to March, when ice concentration is high and almost constant. During this time, we expect variations in thickness to be the primary driver for variations in drift speed. This is clearly the case from December to March (Figure 4b), where the ice thickness increases and speed decreases, while the concentration is constant and high. The anticorrelation between normalized speed and thickness is $\rho = -0.991$ in this period, when averaged over the data-release area and all years.

A similarly strong correlation is found during this period for the northern and southern sections defined in section 3.2.1. In Figure 5b, we have taken the difference in thickness in the different regions into account, but the magnitude of the seasonal cycle in thickness is almost certainly underestimated for the southern section and overestimated for the northern section. This is because the multiple regression model of *Rothrock et al*. [2008] assumes that the seasonal cycle is the same, independent of geographic location. The growth rate of ice is according to Stefan's law, however, proportional to the reciprocal of the thickness [see eg. *Leppäranta*, 1993], while both experience roughly the same melt rate in summer when heat fluxes through the ice become negligible. This leads thick ice showing less seasonality than thin ice, and to the aforementioned underestimation and overestimation. This means that the slope of the graph from December to March will be overestimated in the southern section and underestimated in the northern section. Indeed, a least-squares fit gives a slope of -15 ± 7 (km/d)/(m/s)/m for the southern section, -8.7 ± 3.8 (km/d)/(m/s)/m for the entire area, and -3.1 ± 3.3 (km/d)/(m/s)/m for the northern section. The error estimates of the northern and southern sections do not overlap. Using a correct seasonal cycle in ice growth would bring these values closer together, although it is not clear by how much. We note also that there is no decrease in speed in the northern section from February to March, as opposed to what we see in the southern section and over the entire area.

To examine the impact of a geographically changing seasonal cycle in more detail, we additionally analyze the results of the PIOMAS reanalysis model [*Zhang and Rothrock*, 2003], which has been found to compare reasonably well to the available observations [*Schweiger et al*., 2011]. Figure 6 shows a good agreement between the PIOMAS and the *Rothrock et al*. [2008] model, with slightly thinner ice in the former, particularity in winter. This slight difference does, however, not affect the general relationship between thickness changes and drift speed changes that we examine here.

The most notable difference between the PIOMAS results and the *Rothrock et al*. [2008] model is the shape of the seasonal cycle. *Rothrock et al*. [2008] state that their seasonal cycle is probably not very representative, since it is simply a sinusoidal fit to the data. We therefore expect the shape of the PIOMAS seasonal cycle to be closer to reality. In light of the results of *Rampal et al*. [2011], showing the inability of CMIP3 models to reproduce the seasonal cycle and long-term trend in drift speed, we still believe we should be careful in combining data and model results extensively in this analysis.

Using the PIOMAS seasonal cycle, the increase in speed going from March to June becomes even more pronounced when plotting normalized drift speed against ice thickness. This is because the ice growth during this period is very limited in PIOMAS compared to the *Rothrock et al*. [2008] model. In other respects, there are no qualitative differences between using the PIOMAS and *Rothrock et al*. [2008] thickness; we always find a clear relationship between thickness and normalized drift speed during the high-concentration period from December to March.

3.2.3. April and May

When ice concentration is high, one would expect the ice drift speed to depend on thickness alone, but our analysis indicates a slightly more nuanced picture. From December to March, ice thickness and drift speed are indeed strongly correlated, as one would expect. However, the drift speed increases strongly in April and May, even though both concentration and thickness remain nearly constant. We believe the cause of this to be changes in the fracturing of the ice cover.

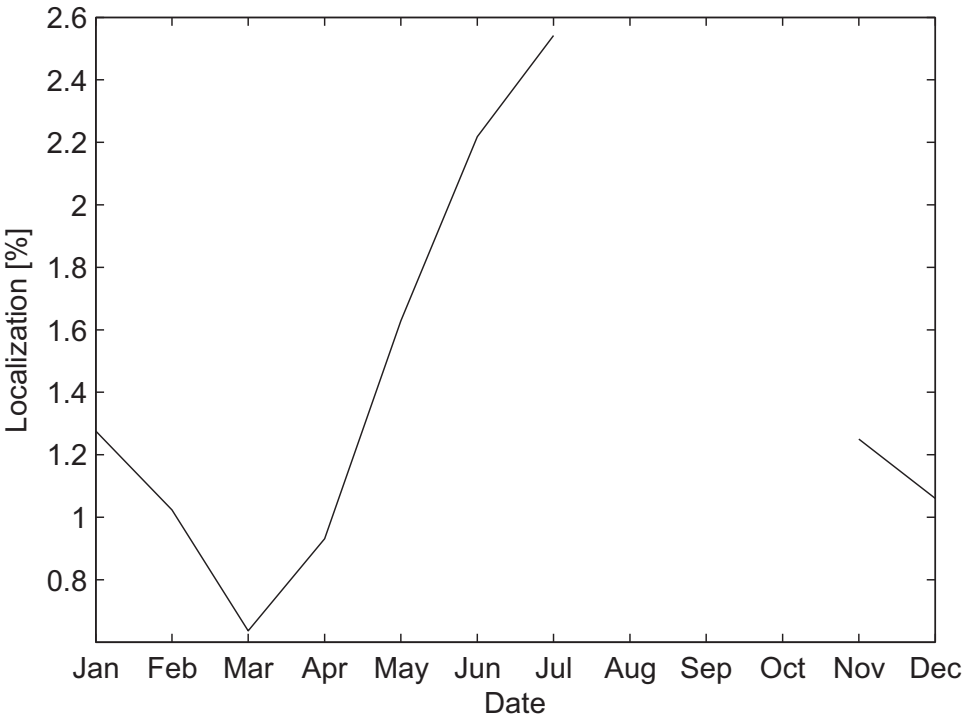

Figure 7. The localization of fractures as the area fraction of the ice which accommodates the largest 15% of the total deformation rate. The localization is calculated over the combined RGPS data record as a function of month from all available RGPS data and from within the data-release area.

We note that the ice thickness increase slows down considerably in April and May, before melt sets in June (assuming the PIOMAS results to be more representative than the *Rothrock et al.* [2008] model). This means also that during these months ice formation over open water is much less than in the preceding months. Once new ice largely stops forming, fractures in the ice will no longer refreeze and the ice cover as a whole looses strength as new fractures form. The ice cover is therefore transformed from a densely packed ice cover that "heals" after a fracture has formed to a densely packed ice cover that grows progressively weaker as new fractures form. As the melting continues, open water forms, and as the fraction of open water increases so does the fraction of sea ice in free drift. When the ice cover closes up again, with the mean concentration approaching one (November), it changes from being in free drift to being compact and healing, without going through an intermediate "weak" state as we propose for April and May.

In order to lend support to this proposed mechanism, we calculate the localization of deformation based on the RGPS data. Using an approach similar to that used by *Marsan et al.* [2004] and *Stern and Lindsay* [2009], we define the total deformation rate

$$\dot{\epsilon}_{tot} = \sqrt{\dot{\epsilon}_{div}^2 + \dot{\epsilon}_{shr}^2}, \tag{3}$$

where $\dot{\epsilon}_{div}$ and $\dot{\epsilon}_{shr}$ are the divergence and shear rates. We then calculate the area fraction of the ice which accommodates the largest 15% of the total deformation rate. In a homogeneous material, this fraction would always be 15%, but it is much lower in sea ice, which has a high degree of deformation localization. A low value for this localization measure indicates a small number of intensely deforming fractures, whereas a large number indicates a large number of less intensely deforming fractures. The localization for each month of the combined RGPS data record is shown in Figure 7.

Our results show a decrease in the localization measure going from November to March, which is consistent with an ice cover that is becoming thicker and more difficult to deform. The localization measure then starts increasing from April to July indicating that a progressively larger number of fractures is opening up and actively deforming during this period. The analysis of *Stern and Lindsay* [2009] of the spatial scaling of Arctic

Table 2. Monthly Trends in Concentration Using the Bootstrap and NASA Team Algorithms[a]

Month	Bootstrap	NASA Team
January	0.02±0.07	**0.53±0.41**
February	0.05±0.06	**0.73±0.31**
March	0.05±0.07	**0.78±0.31**
April	0.05±0.08	**0.34±0.27**
May	0.01±0.05	−0.31±0.33
June	**−0.27±0.25**	**−1.12±0.84**
July	**−1.50±0.58**	**−2.81±1.30**
August	**−4.12±1.21**	**−5.44±2.04**
September	**−3.16±0.79**	**−4.52±1.70**
October	**−2.76±1.24**	**−3.98±1.90**
November	−0.20±0.23	−0.39±0.81
December	−0.02±0.09	0.11±0.63

[a]Units for concentration are %/decade. The error shown is the accompanying 95% confidence limit and statistically significant trends are written in bold.

sea-ice deformation shows that the ice cover remains very compact until mid-May, when it starts loosening up (see also the discussion in section 5). This shows that in April and early May the ice cover is very compact, while the number of fractures is increasing. This is a strong indication that the increased movement of the ice in April and May is due to increased number of active leads, which stay active due to their inability to refreeze.

Our explanation is closely related to that which *Gimbert et al*. [2012a, 2012b] use to explain the discrepancy between their model results and the conventional view of sea-ice dynamics. They suggest that mechanical weakening through increased fracturing may be responsible for weakening unrelated to ice thickness and concentration. In our view, fracturing of the ice does indeed play a role, but it is not increased fracturing as such, but rather the fracture's inability to refreeze that matters most.

4. Long-Term Trend

We now turn to long-term trends in the monthly mean ice drift speed, and compare them to trends in the observed concentration and thickness. We consider the trends over periods during which we have already shown seasonal changes in concentration and thickness to influence drift speed. We expect there to be a similar trend in thickness for all months [cf., *Rothrock et al*., 2008; *Schweiger et al*., 2011], so we consider the combined trend for the months from December through March to represent the months where drift-speed variations are primarily controlled by thickness variations. The trend in concentration is, however, strongest during August, September, and October (see Table 2) and we accordingly consider the trend in drift speed for these months collectively (Figure 8). The trends were found using a nonlinear least-squares algorithm, weighted appropriately with the errors from the bootstrap method (although this is probably an overestimation of the error). The errors reported on the trend are the 95% confidence limit resulting from a χ^2-test.

The drift-speed trend in August–October is 1.1 ± 0.3 km/d/decade, the largest of any three or more consecutive months. The trend for December–March is considerably smaller, at 0.4 ± 0.3 km/d/decade. The trend in drift speed for the transition months of April and May is not significant and the trend for the period June–November is 0.5 ± 0.2 km/d/decade. We therefore consider the bulk of the trend to be found in the period August–October, coinciding with the observed negative trend in concentration. We also show the December–March mean drift speed from the satellite observations in Figure 8. This has a trend of 0.5 ± 0.3 km/d/decade and is biased slow compared to the buoy-based time series.

It is worth noting that this result does not contradict that of *Rampal et al*. [2009] who report that trends in winter are similar to those in summer. This is because *Rampal et al*. [2009] define winter as lasting from 1 December to 15 May and summer from 15 June to 30 September. The trends in January and April are therefore included in their winter average, but the trends in October and November are excluded from their summer average, leading to similar trends for the two seasons thus defined. There seems to be a general tendency in the literature to equate summer roughly with the melt period and winter with the freeze up [cf., *Rampal et al*., 2009; *Spreen et al*., 2011; *Kwok et al*., 2013]. Our results, however, indicate that it is also useful to consider seasons defined based on the kinematics of the ice cover, not only on the thermodynamics, as e.g., *Stern and Moritz* [2002] have done.

Using the same arguments as before, the trends in drift speed can be traced to one or more of three factors: a possible trend in wind forcing, a trend in ice thickness, or a trend in ice concentration. Assuming the weakening, we observe in April and May is due to increased fracturing, we would not expect a strong trend in those months. Note, however, that changes in the timing of the onset of melt could affect trends in these months.

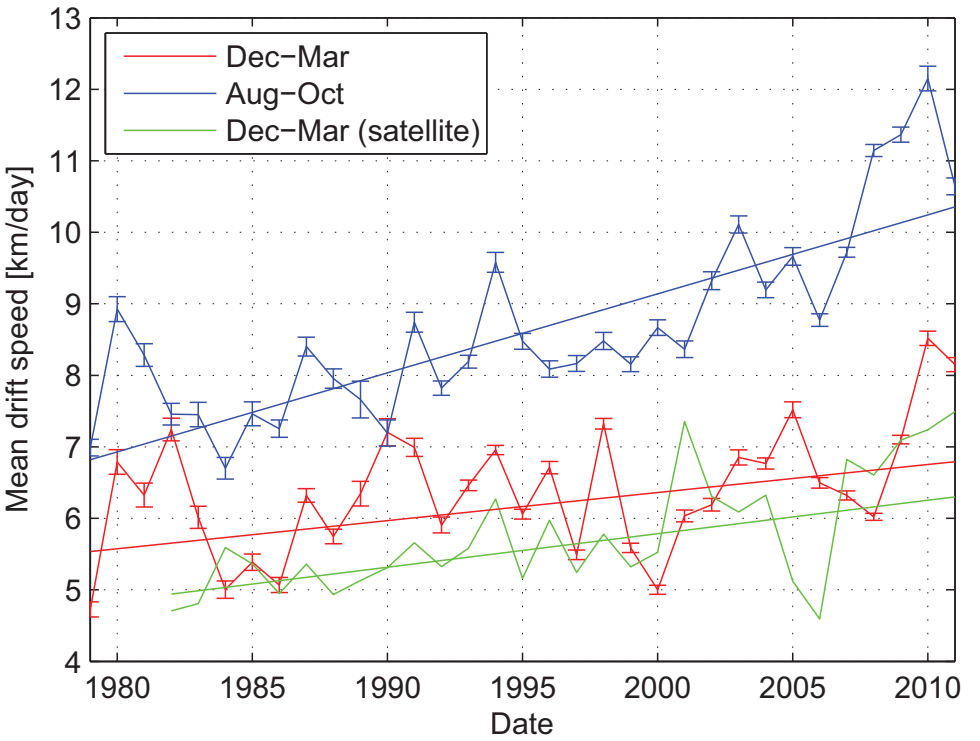

Figure 8. Time series and linear trends of monthly mean drift speed for December–March and August–October based on buoy displacements as well as the December–March time series and trend from the satellite-based product. All are averaged over the submarine data release area. The error bars show error estimates derived using the bootstrap method, as described in the text.

We found no significant trends in the ERA-interim reanalysis wind speed, thus ruling out a trend in the forcing as a significant effect. *Rampal et al.* [2009] come to the same conclusion, and while *Spreen et al.* [2011] do find a role of wind forcing in driving an increase in drift speed, they find this to be mostly limited to the first decade of the 21st century. *Vihma et al.* [2012] consider the relationship between sea-ice drift speed and various atmospheric indices for the period 1989–2009 concluding that atmospheric forcing does not explain the increasing trend in drift speed for that period.

This leaves a long-term trend in concentration or thickness as the most likely major driving factor for the trend in drift speed. During the period, December–March concentration is high with a small or insignificant trend in our area of interest. We can therefore expect the trend in drift speed to be caused by a thinning of the ice during these months. During the period 1979–2000, the *Rothrock et al.* [2008] multiple regression model shows a thinning trend of 0.60 m/decade while the ICESat record shows a thinning of 1.0 m/decade in winter from 2003 to 2008 [*Kwok and Rothrock*, 2009]. For comparison, the PIOMAS model gives a considerably smaller thinning trend of 0.25 m/decade in winter for the 1979–2010 period [*Schweiger et al.*, 2011]. Overall *Kwok and Rothrock* [2009] state that the peak winter mean thickness of the ice within the submarine data-release area has decreased from 3.64 m in 1980 to 1.89 m by winter 2008, a decrease of 1.75 m. This gives a mean decrease of 0.60 m/decade, the same as the trend of the multiple regression model. This decrease in thickness is nearly double the seasonal increase in thickness from December to March and should consequently be capable of driving a considerable increase in drift speed.

During the period, August–October concentration is relatively low and we expect the observed trend in concentration to be the main driver of the trend in drift speed, analogous to what we have already seen in the seasonal cycle. Filtering out the synoptic-scale forcing by analyzing long-term trends in the fortnightly data, the August–October trend remains significant, but is reduced to 0.6 ± 0.3 km/d/decade, from 1.1 ± 0.3 km/d/decade. It is therefore reasonable to assume that the August–October trend is largely driven by increased synoptic-scale response through lowered concentration, similarly to what we found before for the seasonal cycle.

Seeing that the August–October trend in drift speed is largely due to increased ice movement on the synoptic scale, one could argue that the trend may be caused by a positive trend in cyclone activity. *McCabe et al*. [2001]; *Zhang et al*. [2004]; and *Sepp and Jaagus* [2011] all find that cyclone activity in the Arctic has increased in the last decades, and they also find that the increase is mostly uniform throughout the year. The possible impact of this finding will be discussed in a somewhat greater detail in the following section.

It should also be noted that our analysis may underestimate the trend in drift speed from December to March. The main reason for this is that the buoys are preferentially placed on thick or multiyear ice. This masks the impact of multiyear ice loss on increased drift speed, which *Kwok et al*. [2013] find to be important. However, the velocity fields derived from SSM/I, SSMIS, and AVHRR data show a trend of 0.5 $\pm$ 0.3 km/d/decade for the months of December–March, only slightly larger than the 0.4 $\pm$ 0.3 km/d/decade derived from the buoys. This indicates that the regional effects reported by *Kwok et al*. [2013] are currently not strong enough to have Arctic-wide long-term effects. This is reasonable given that the loss of multiyear ice and the associated increase in drift speed has occurred primarily regionally and in the 21st century [see Figures 3 and 6 of *Kwok et al*., 2013]. Our results do not contradict those of *Kwok et al*. [2013] since we find a strong relationship between drift speed and thickness which we expect to cause a considerable increase in drift speed where multiyear ice is replaced by much thinner first-year ice.

5. Discussion

In this paper, we have studied the spatially averaged central Arctic drift speed as recorded by IABP buoys. Our focus has been twofold: first, to identify the drivers shaping the observed seasonal cycle, and second to identify those behind the observed long-term trend. In this section, we will discuss the most interesting aspects of our results in more detail.

Our analysis shows that seasonal variations in ice concentration and thickness are correlated with variations in drift speed, and that variations in wind speed and cyclone activity are unlikely to have a substantial effect. Variations in drift speed and concentration are correlated from June to November, as concentration decreases and increases again. This is to be expected since we know that loose ice moves more easily than compact ice, but we believe that this relationship has not been demonstrated explicitly at the large scale before.

Having analyzed the seasonal cycle in drift speed, we moved to the observed long-term trend in drift speed. We found that this is strongest during August, September, and October, which we show to be partially influenced by synoptic-scale forcing. The drift-speed trend in August–October coincides with a negative trend in concentration. There is also a small, but significant trend in drift speed from December to March, which we relate to a trend in ice thickness.

Our results compare relatively well with those of *Thomas* [1999], who considered the linear relationship between ice drift and geostrophic winds:

$$U = AG + D + E, \tag{4}$$

where U is the complex ice velocity, G the geostrophic wind, A and D are constants determined from the data, and E is the residual. A high correlation coefficient between U and G indicates that much of the ice is in free drift. *Thomas* [1999] found that the correlation coefficient between U and G showed a weak seasonal cycle, one that is consistent with our results. He also found the relationship between the seasonal cycle of the absolute value of A and its angle to allow him to better define a seasonal cycle, stating that the data "suggests a summer of June through September, and a winter of November through April, with May and October being intermediate "transition" months" [*Thomas*, 1999, p. 13,630]. This timing is mostly consistent with our results, but we note that both approaches leave some room for interpretation and that *Thomas* [1999] uses geostrophic winds based on the observed pressure field while we use surface wind stress from a reanalysis.

We can also relate our results to the results of *Stern and Lindsay* [2009] on spatial scaling of Arctic sea ice deformation that show how the power-law scaling exponent changes seasonally. This exponent is mostly constant from November to mid-May when it starts to decrease until the start of August. No RGPS data are available in August, September, and October. *Stern and Lindsay* [2009] interpret this decrease of the exponent as a signature of the ice pack loosening up, since the decreasing exponent shows that stresses are not

transmitted as readily through the ice pack as before. This estimate of the ice pack starting to break up in May fits reasonably well with our conclusion that changes in concentration start affecting changes in drift speed in June. Note that the RGPS data does not cover the entire central Arctic and that this may lead to an early bias in the results of *Stern and Lindsay* [2009] compared to ours.

In another related study, *Zhang et al*. [2012] used the PIOMAS model to examine some of the relationships that we have discussed here. The model captures the seasonality in drift speed quite well, with a reasonable minimum in May and maximum in October. The authors relate this to a seasonal cycle in ice strength, which depends on both the ice thickness and concentration, without attempting to separate the influence of these two factors on the ice strength. The increase in drift speed observed from April to May is, however, not present in the model results. This is consistent with the speed increase being caused by an increased number of active fractures, since the ice strength in the PIOMAS model only depends on ice concentration and thickness. The model shows a long-term increase in drift speed (calculated as the difference between the 2007–2011 and 1979–2006 means), with the largest increase in October and November and almost no increase in August and September. This contradicts the observations, which show the largest long-term trend to occur in August–October. The PIOMAS model therefore shows promise, but fails to capture some of the more interesting features found in the observations.

Using our results, we can now estimate how much the observed trends in concentration and thickness contribute to the trends in drift speed. To do this, we assume that the linear relationships we found between normalized drift speed and concentration and normalized drift speed and thickness on the seasonal time scale to hold in general. Starting with the relationship between concentration and normalized drift speed from June to November, a linear fit to the data gives a change of -64 ± 41 (km/d)/(m/s) in normalized drift speed for a unit change in Bootstrap-derived ice concentration. The mean long-term trend in concentration in August–October is -6.3%/decade and the mean friction speed is 0.25 m/s. This gives a resulting change in drift speed of 1.0 km/d/decade caused by the change in concentration. This is very close to the observed 1.1 ± 0.3 km/d/decade, indicating that the trend in drift speed is almost entirely caused by the trend in concentration. However, if we use the results from the NASA Team algorithm (with a slope of -25 ± 23 (km/d)/(m/s) per unit change in concentration and a mean trend of -7.8 %/decade), we estimate the trend in drift speed caused by the trend in concentration to be only 0.5 km/d/decade. Should this hold, a substantial portion of the trend in drift speed is caused by a different process, most likely a trend in cyclone activity. We have so far preferred the Bootstrap algorithm and expect the results based on it to be more representative. One can, however, also argue in favor of the NASA Team algorithm, seeing it gives concentration more in line with the other algorithms shown in Figure 6. We can therefore not state with confidence to which extent the trend in concentration drives the trend in drift speed, only that it does so to a substantial amount.

We can also estimate the contribution of the trend in ice thickness to the trend in drift speed in December–March using the slope of the linear fit between thickness, derived from submarine observations and normalized drift speed. In this case, the slope is -8.7 ± 3.8 (km/d)/(m/s)/m and the mean friction speed is again 0.25 m/s. We have already discussed estimates of the observed trend, based on *Rothrock et al*. [2008] and *Kwok and Rothrock* [2009] and 0.60 m/decade appears to be reasonable. This trend should then drive a trend in drift speed of 1.4 km/d/decade. This is substantially larger than the observed trend of 0.4 ± 0.3 km/d/decade, indicating that the relationship between drift speed and thickness is more complex than we have assumed. This could mean that any of the factors that we neglected is more important than we have assumed, including changes in atmospheric or oceanic drag, or stratification, or changes in ocean currents possibly being important. If we use, however, the trend from the PIOMAS model, which is 0.25 m/decade then that trend should drive a drift-speed trend of 0.54 km/decade, which is much closer to the observed value.

It is difficult to estimate the thickness trend, based on observations and it is possible that this trend is overestimated in the *Rothrock et al*. [2008] multiple regression model. *Schweiger et al*. [2011] find that the PIOMAS trends are probably somewhat smaller than the actual trend, although their analysis indicates that 0.60 m/decade is likely a considerable overestimation. Based on that we find it likely that the relationship between drift speed and thickness we have used holds and that the trend in drift speed from December to March is driven almost solely by a trend in thickness.

Finally we note the importance of the synoptic-scale movement when comparing model results and observations. In particular, the CMIP3 archive only includes monthly averaged u and v ice velocity components,

which hence loses the significant synoptic impact on ice drift-speed. This makes the archived data unsuitable for direct comparison with observations of 12 hourly averaged displacements. One should therefore not expect the archived CMIP3 data to show a strong seasonal cycle or long-term trend in drift speed, even if they were present in the original models. Hence, much of the difference between the seasonal cycle and long-term trend in CMIP3 models and observations that were found by *Rampal et al*. [2011] might stem from the difference in averaging periods.

6. Conclusions

Based on an analysis of seasonal variations, we find that changes in the ice drift-speed are primarily driven by either changes in thickness or concentration. While this has generally been known before, we here show explicitly that this behavior indeed holds for the Arctic as a whole. In particular, we reach the following conclusions regarding the seasonal cycle:

1. On the seasonal time scale, changes in concentration are the primary driver of changes in drift speed, through changes in the ice cover's sensitivity to synoptic-scale forcing in the atmosphere. This effect is prevalent from June to November.
2. On the seasonal time scale, changes in ice thickness are the primary driver of changes in drift speed only when mean concentration is constantly very high, i.e., from December to March.
3. April and May see an increase in drift speed, unrelated to changes in concentration or thickness. We show that this coincides with increased fracturing of the ice cover and propose that this is due to its inability to refreeze after fracturing events.

We have also determined that the observed long-term trend in drift speed is largely caused by a long-term trend in ice concentration. In particular, our conclusions regarding the long-term trend in drift speed are:

1. A long-term trend in drift speed from August to October is likely primarily caused by a negative trend in concentration, possibly reinforced by a trend in cyclone activity.
2. Roughly half the trend in drift speed in August–October is driven by an increased response to synoptic forcing, realized because of the decreasing concentration. This portion does therefore not necessarily imply an increase in ice area export.
3. A weaker long-term trend in drift speed from December to March is likely primarily caused by the thinning of the ice.

Finally we note that the importance of synoptic-scale movement hinders a direct comparison of observations with the archived CMIP3 drift speed. Such variability in ice movement is lost in the archived data because only monthly averages of the velocity components were stored, not monthly averaged speed.

Appendix A: Filling the Pole Hole

A peculiarity of the satellite data is the so-called "pole hole," a circular region around the pole not covered by the satellite observations (see Figure 1). The first observations from 1979 to August 1987 only reached 84.5°N while after that they reached 87.2°N. When using ice concentrations produced with the Bootstrap algorithm, the pole hole can be filled with a constant value without significantly impacting our results. The other algorithms used here give too high variability in the central Arctic for this approach to be viable. We fill the hole with the mean concentration of the outer rim of the large pole hole (i.e., between 84.5°N and 87.2°N), from August 1987 onward. This mean value is $\bar{A}=0.988$, with a standard deviation of 0.006, no significant trend and a small seasonal cycle compared to the standard deviation (see Figure 9). The only significant deviations from this mean value (within the 95% confidence limit) were 1–2 month-long extreme events in 1991, 1996, 2007, and 2010.

To test the effects of filling the pole holes in this manner, we repeated the relevant calculations, both excluding the pole hole and with it being filled with $\bar{A}=1$. The results remained qualitatively the same and the quantitative differences remained within the resulting error margins. The pole holes therefore have little significance for our concentration calculations when using data based on the Bootstrap algorithm, but it is important not to have to exclude the pole holes from the other data sets.

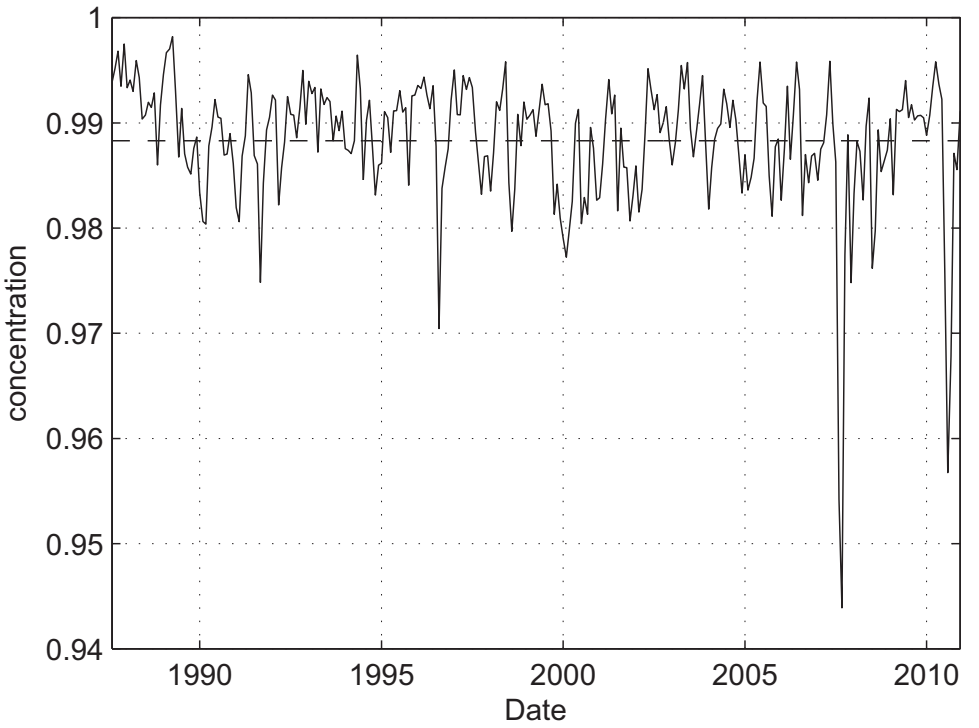

Figure 9. Mean concentration from within the outer rim of the large pole hole. The dashed line shows the temporal mean.

Appendix B: Analysis of Ice Drift Speed From Satellite Observations

The ice drift speed derived from satellite observations used here is that provided by *Fowler et al*. [2013]. These are ice drift vectors derived from satellite imagery using the maximum cross-correlation techniques of *Emery et al*. [1995]. Table 3 lists the sensors used and the time period over which the data are available. Note that *Fowler et al*. [2013] provide data from the SMMR, SSM/I, and SSMIS sensors as a single data set under the label "SSMI," and we use this nomenclature here too, unless otherwise stated. *Fowler et al*. [2013] also provide a merged product which uses optimal interpolation to combine the aforementioned drift vectors with buoy drift vectors and ice motion vectors derived from NCEP/NCAR reanalysis wind fields, assuming a drag coefficient and a turning angle. The merged product provides daily, Arctic wide drift-speed fields from 1 November 1978 onward, on a 25 km resolution EASE-grid. In order to better understand the characteristics of this data, we calculate the seasonal cycle and December–March long-term trends for each of the sensors and the merged product inside the submarine data-release area.

Starting with the seasonal cycle of drift speed, Figure 10 shows the seasonal cycles from the three drift vector data sets as well as the merged product, compared with the seasonal cycle already derived from the buoys. From this figure, it is clear that the merged product and the SSMI and AVHRR data sets underestimate the drift speed compared to the buoys, while the AMSR-E data set shows speeds that compare much better with the buoy speeds. We note also that the SSMI and merged data sets show a speed decrease in summer, not an increase, like the buoy data. The AMSR-E data generally agrees with the buoy data, except for the months of August and September when the speed is underestimated, compared to the buoys. The AVHRR data appear to underestimate the drift speed in June and July but has otherwise a reasonably well-shaped seasonal cycle. Due to the overall

Table 3. Satellite Sensors Used in the Merged Drift-Speed Product

Sensor(s)	Data Period
SMMR	1 November 1978–31 July 1987
SSM/I	1 August 1987–31 October 2005
SSMIS	1 November 2005 to the present
AVHRR	24 July 1981–31 December 2000
AMSR-E	19 June 2002–8 August 2011

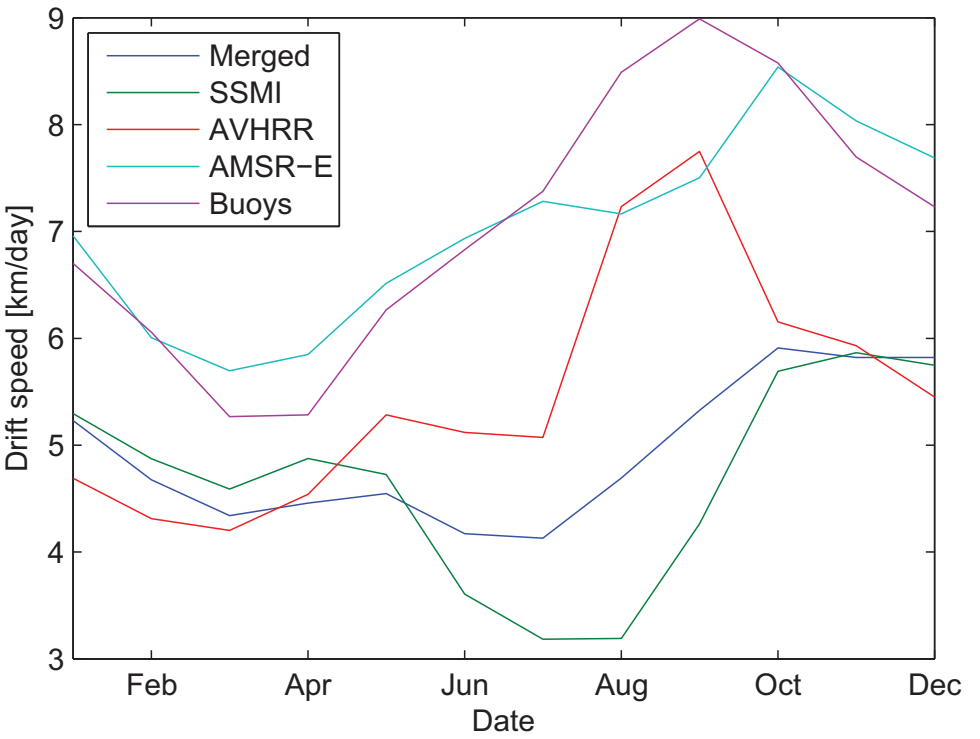

Figure 10. The seasonal cycle of drift speed derived from buoy motion, the merged data set, and three of its components. All are averaged over the submarine data release area and all available years.

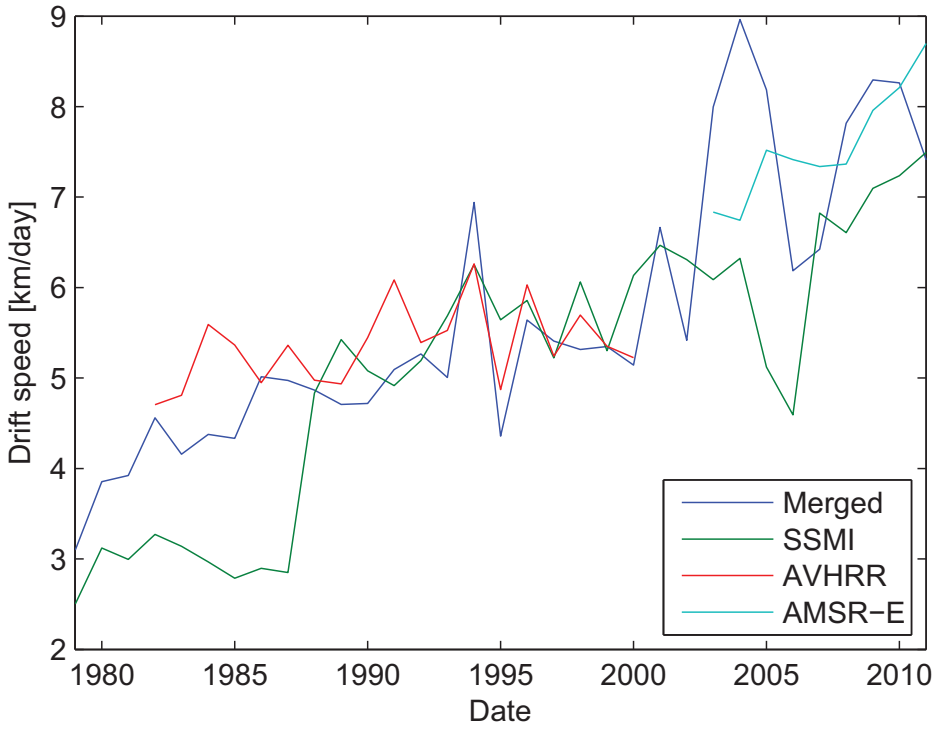

Figure 11. Time series of the mean drift speed in December–March derived from the merged data set and three of its components.

poor performance of the satellite products in summer, we choose to focus on the period December–March for the long-term trend analysis.

We next calculate the time series of mean December–March drift speed for each sensor and the merged data set (Figure 11). This shows two important inconsistencies in the data. First, the SSMI data set shows a very sharp increase in speed going from 1987 to 1988, which coincides with a switch from the SMMR sensor to SSM/I. Comparing the SSMI time series with that derived from the AVHRR data, it is clear that the SMMR-based portion of the SSMI time series severely underestimates the drift speed. A possible reason for this is that the SMMR images are only available every other day. As a result of this, the drift speed of the merged data set is too low during the SMMR period. The second inconsistency to note is that the AMSR-E derived drift speeds are considerably higher than the SSMI drift speeds. We have already seen that the SSMI drift speeds are probably biased low and that the AMSR-E speeds are closer to being correct. However, since the bulk of the merged data set is based on the SSMI data, introducing the AMSR-E data introduces an artificial speed increase toward the end of the time series into the merged data set.

Based on these observations, it is clear that simply calculating the drift-speed trend of the merged product will give a considerable overestimation of the actual trend. Instead, we use a combination of the AVHRR data and the SSMI time series from after 1987 (coinciding with use of the SSM/I and SSMIS sensors), where we again treat each drift vector provided as an independent observation.

Acknowledgments

We would like to thank Philipp Griewank and Stefan Kern for helpful comments and suggestions which helped improving this paper. We would also like to thank Florent Gimbert, Pierre Rampal, and Roger Colony for their comments on earlier versions of this paper and for helpful discussions. We would also like to thank the anonymous reviewers, who's comments helped to greatly improve the paper. ASI Algorithm SSMI-SSMIS, AMSR-E and MPF sea ice concentrations were obtained from the Integrated Climate Data Center (ICDC, http://icdc.zmaw.de/), University of Hamburg, Hamburg, Germany, June 2013.

References

Brümmer, B., and H. Hoeber (1999), A mesoscale cyclone over the Fram strait and its effects on sea ice, *J. Geophys. Res.*, *104*(D16), 19,085–19,098, doi:10.1029/1999JD900259.

Colony, R., and A. S. Thorndike (1984), An estimate of the mean field of Arctic sea ice motion, *J. Geophys. Res.*, *89*(C6), 10,623–10,629, doi:10.1029/JC089iC06p10623.

Comiso, J. (2000), *Bootstrap Sea Ice Concentrations from Nimbus-7 SMMR and DMSP SSM/I-SSMIS*, Natl. Snow and Ice Data Cent., Boulder, Colo., version 2, updated 2012.

Comiso, J. C., and C. L. Parkinson (2008), Arctic sea ice parameters from AMSR-E data using two techniques and comparisons with sea ice from SSM/I, *J. Geophys. Res.*, *113*, C02S05, doi:10.1029/2007JC004255.

Coon, M., R. Kwok, G. Levy, M. Pruis, H. Schreyer, and D. Sulsky (2007), Arctic Ice Dynamics Joint Experiment (AIDJEX) assumptions revisited and found inadequate, *J. Geophys. Res.*, *112*, C11S90, doi:10.1029/2005JC003393.

Coon, M. D., G. A. Maykut, R. S. Pritchard, D. A. Rothrock, and A. S. Thorndike (1974), Modeling the pack ice as an elastic-plastic material, *AIDJEX Bull.*, *24*, 1–105.

Ekman, V. W. (1904), On dead water, in *The Norwegian North Polar Expedition 1893–1896: Scientific Results*, vol. V, edited by F. Nansen, pp. 1–152, Copp. Clark, Mississauga, Ont.

Emery, W., C. Fowler, and J. Maslanik (1995), Satellite remote sensing of ice motion, in *Oceanographic Applications of Remote Sensing*, edited by M. Ikeda and F. W. Dobson, CRC Press, Boca Raton, Fla.

Fowler, C., W. Emery, and M. Tschudi (2013), *Polar Pathfinder Daily 25 km EASE-Grid Sea Ice Motion Vectors*, version 2, Natl. Snow and Ice Data Cent., Boulder, Colo.

Gimbert, F., N. C. Jourdain, D. Marsan, J. Weiss, and B. Barnier (2012a), Recent mechanical weakening of the Arctic sea ice cover as revealed from larger inertial oscillations, *J. Geophys. Res.*, *117*, C00J12, doi:10.1029/2011JC007633.

Gimbert, F., D. Marsan, J. Weiss, N. C. Jourdain, and B. Barnier (2012b), Sea ice inertial oscillations in the Arctic Basin, *Cryosphere*, *6*(5), 1187–1201, doi:10.5194/tc-6-1187-2012.

Gordienko, P. (1958), Arctic ice drift, in *Arctic Sea Ice: Proceedings of the Conference*, edited by M. Easton, pp. 210–220, Natl. Acad. Sci., Natl. Res. Counc., Washington, D. C.

Hibler, W. D. (1979), A dynamic thermodynamic sea ice model, *J. Phys. Oceanogr.*, *9*(4), 815–846, doi:10.1175/1520-0485(1979)009<0815:ADTSIM >2.0.CO;2.

Hibler, W. D. (1980), Modeling a variable thickness sea ice cover, *Mon. Weather Rev.*, *108*(12), 1943–1973, doi:10.1175/1520-0493(1980)108<1943:MAVTSI >2.0.CO;2.

Holt, B., and S. Martin (2001), The effect of a storm on the 1992 summer sea ice cover of the Beaufort, Chukchi, and East Siberian Seas, *J. Geophys. Res.*, *106*(C1), 1017–1032, doi:10.1029/1999JC000110.

Hopkins, M. A. (1998), Four stages of pressure ridging, *J. Geophys. Res.*, *103*(C10), 21,883–21,891, doi:10.1029/98JC01257.

Kaleschke, L., C. Lüpkes, T. Vihma, J. Haarpaintner, A. Bochert, J. Hartmann, and G. Heygster (2001), SSM/I sea ice remote sensing for mesoscale ocean-atmosphere interaction analysis, *Can. J. Remote Sens.*, *27*(5), 529–537.

Kwok, R., and D. A. Rothrock (2009), Decline in Arctic sea ice thickness from submarine and ICESat records: 1958–2008, *Geophys. Res. Lett.*, *36*, L15501, doi:10.1029/2009GL039035.

Kwok, R., J. C. Curlander, R. McConnell, and S. S. Pang (1990), An ice-motion tracking system at the Alaska SAR facility, *IEEE J. Oceanic Eng.*, *15*(1), 44–54.

Kwok, R., G. Spreen, and S. Pang (2013), Arctic sea ice circulation and drift speed: Decadal trends and ocean currents, *J. Geophys. Res. Oceans*, *118*, 2408–2425, doi:10.1002/jgrc.20191.

Leppäranta, M. (1993), A review of analytical models of sea-ice growth, *Atmos. Ocean.*, *31*(1), 123–138, doi:10.1080/07055900.1993.9649465.

Leppäranta, M. (2005), *The Drift of Sea Ice*, pp. 130–133, Springer-Verlag, Berlin Heidelberg, N. Y.

Lipscomb, W. H., E. C. Hunke, W. Maslowski, and J. Jakacki (2007), Ridging, strength, and stability in high-resolution sea ice models, *J. Geophys. Res.*, *112*, C03S91, doi:10.1029/2005JC003355.

Lu, P., Z. Li, B. Cheng, and M. Leppranta (2011), A parameterization of the ice-ocean drag coefficient, *J. Geophys. Res.*, *116*, C07019, doi:10.1029/2010JC006878.
Lüpkes, C., V. M. Gryanik, A. Rsel, G. Birnbaum, and L. Kaleschke (2013), Effect of sea ice morphology during arctic summer on atmospheric drag coefficients used in climate models, *Geophys. Res. Lett.*, *40*, 446–451, doi:10.1002/grl.50081.
Markus, T., and D. Cavalieri (2000), An enhancement of the NASA Team sea ice algorithm, *IEEE Trans. Geosci. Remote Sens.*, *38*(3), 1387–1398, doi:10.1109/36.843033.
Marsan, D., H. Stern, R. Lindsay, and J. Weiss (2004), Scale dependence and localization of the deformation of arctic sea ice, *Phys. Rev. Lett.*, *93*(17), 178501.
Martin, T., and R. Gerdes (2007), Sea ice drift variability in Arctic Ocean Model Intercomparison Project models and observations, *J. Geophys. Res.*, *112*, C04S10, doi:10.1029/2006JC003617.
Maslanik, J. A., and R. Barry (1989), Short-term interactions between atmospheric synoptic conditions and sea-ice behavior in the Arctic, *Ann. Glaciol.*, *12*, 113–117.
McCabe, G. J., M. P. Clark, and M. C. Serreze (2001), Trends in northern hemisphere surface cyclone frequency and intensity, *J. Clim.*, *14*(12), 2763–2768, doi:10.1175/1520-0442(2001)014<2763:TINHSC >2.0.CO;2.
Meier, W., and D. Notz (2010), A note on the accuracy and reliability of satellite-derived passive microwave estimates of sea-ice extent, in *CliC Arctic Sea Ice Working Group Consensus Document*, pp. 1–4, World Climate Research Program, The Climate and Cryosphere (CliC), Tromso, Norway.
Proshutinsky, A. Y., and M. A. Johnson (1997), Two circulation regimes of the wind-driven Arctic Ocean, *J. Geophys. Res.*, *102*(C6), 12,493–12,514, doi:10.1029/97JC00738.
Rampal, P., J. Weiss, and D. Marsan (2009), Positive trend in the mean speed and deformation rate of Arctic sea ice, 1979–2007, *J. Geophys. Res.*, *114*, C05013, doi:10.1029/2008JC005066.
Rampal, P., J. Weiss, C. Dubois, and J.-M. Campin (2011), IPCC climate models do not capture Arctic sea ice drift acceleration: Consequences in terms of projected sea ice thinning and decline, *J. Geophys. Res.*, *116*, C00D07, doi:10.1029/2011JC007110.
Rösel, A., L. Kaleschke, and G. Birnbaum (2012), Melt ponds on Arctic sea ice determined from MODIS satellite data using an artificial neural network, *Cryosphere*, *6*(2), 431–446, doi:10.5194/tc-6-431-2012.
Rothrock, D. A. (1975), The energetics of the plastic deformation of pack ice by ridging, *J. Geophys. Res.*, *80*(33), 4514–4519, doi:10.1029/JC080i033p04514.
Rothrock, D. A., D. B. Percival, and M. Wensnahan (2008), The decline in arctic sea-ice thickness: Separating the spatial, annual, and interannual variability in a quarter century of submarine data, *J. Geophys. Res.*, *113*, C05003, doi:10.1029/2007JC004252.
Schweiger, A., R. Lindsay, J. Zhang, M. Steele, H. Stern, and R. Kwok (2011), Uncertainty in modeled Arctic sea ice volume, *J. Geophys. Res.*, *116*, C00D06, doi:10.1029/2011JC007084.
Sepp, M., and J. Jaagus (2011), Changes in the activity and tracks of Arctic cyclones, *Clim. Change*, *105*(3-4), 577–595, doi:10.1007/s10584-010-9893-7.
Simmons, A. J., S. M. Uppala, D. P. Dee, and S. Kobayashi (2006), ERA-interim: New ECMWF reanalysis products from 1989 onwards, *ECMWF Newsl.*, *110*, 26–35.
Spreen, G., L. Kaleschke, and G. Heygster (2008), Sea ice remote sensing using AMSR-E 89-GHz channels, *J. Geophys. Res.*, *113*, C02S03, doi:10.1029/2005JC003384.
Spreen, G., R. Kwok, and D. Menemenlis (2011), Trends in Arctic sea ice drift and role of wind forcing: 1992–2009, *Geophys. Res. Lett.*, *38*, L19501, doi:10.1029/2011GL048970.
Stern, H. L., and R. W. Lindsay (2009), Spatial scaling of Arctic sea ice deformation, *J. Geophys. Res.*, *114*, C10017, doi:10.1029/2009JC005380.
Stern, H. L., and R. E. Moritz (2002), Sea ice kinematics and surface properties from RADARSAT synthetic aperture radar during the SHEBA drift, *J. Geophys. Res.*, *107*(C10), 8028, doi:10.1029/2000JC000472.
Thomas, D. (1999), The quality of sea ice velocity estimates, *J. Geophys. Res.*, *104*(C6), 13,627–13,652, doi:10.1029/1999JC900086.
Thorndike, A. S., and R. Colony (1982), Sea ice motion in response to geostrophic winds, *J. Geophys. Res.*, *87*(C8), 5845–5852, doi:10.1029/JC087iC08p05845.
Vihma, T., P. Tisler, and P. Uotila (2012), Atmospheric forcing on the drift of Arctic sea ice in 1989–2009, *Geophys. Res. Lett.*, *39*, L02501, doi:10.1029/2011GL050118.
Waters, J. K., and M. S. Bruno (1995), Internal wave generation by ice floes moving in stratified water: Results from a laboratory study, *J. Geophys. Res.*, *100*(C7), 13,635–13,639, doi:10.1029/95JC01220.
Zhang, J., and D. A. Rothrock (2003), Modeling global sea ice with a thickness and enthalpy distribution model in generalized curvilinear coordinates, *Mon. Weather Rev.*, *131*(5), 681–697.
Zhang, J., R. Lindsay, A. Schweiger, and I. Rigor (2012), Recent changes in the dynamic properties of declining Arctic sea ice: A model study, *Geophys. Res. Lett.*, *39*, L20503, doi:10.1029/2012GL053545.
Zhang, X., J. E. Walsh, J. Zhang, U. S. Bhatt, and M. Ikeda (2004), Climatology and interannual variability of Arctic cyclone activity: 1948–2002, *J. Clim.*, *17*, 2300–2317, doi:10.1175/1520-0442(2004)017<2300:CAIVOA >2.0.CO;2.
Zwally, H. J., and J. E. Walsh (1987), Comparison of observed and modeled ice motion in the Arctic Ocean, *Ann. Glaciol.*, *9*, 136–144.